Visible to Mid-Infrared Photodetection Based on Flexible 3D Graphene/Organic Hybrid Photodetector with Ultrahigh Responsivity at Ambient Conditions

Zhen Ge, Nuo Xu, Yu Zhu, Kai Zhao, Yanfeng Ma, Guanghui Li,* and Yongsheng Chen*

Cite This: *ACS Photonics* 2022, 9, 59−67

Read Online

ACCESS | Metrics & More | Article Recommendations | SI Supporting Information

ABSTRACT: Near-infrared (NIR) and mid-infrared (MIR) photodetectors have wide applications in biometrics, military, industry, etc. NIR and MIR organic photodetectors (OPD) require narrow-bandgap semiconductors to achieve efficient light absorption. However, it is still a challenge to synthesize organic materials with efficient absorption region above 1000 nm. Herein, a flexible hybrid OPD has been designed and fabricated by integrating organic materials with three-dimensional graphene (3DG) film, and the photodetector can detect light from visible to MIR at room temperature with an outstanding responsivity of 108 A W^{-1} in the NIR region (1000 nm). Moreover, the hybrid device can detect picowatt-level light with ultrahigh responsivity of 5.8×10^5 A W^{-1} and specific detectivity of 3×10^{15} Jones in the visible region. Furthermore, the 3DG film/organic hybrid detector is well compatible with flexible substrates and opens up a novel approach to developing flexible photodetectors with high responsivity in a wide spectrum range, suggesting possible potential applications in flexible electronics.

KEYWORDS: *NIR and MIR photodetector, 3D graphene, organic photodetector, flexible photodetector, long-wavelength photodetector*
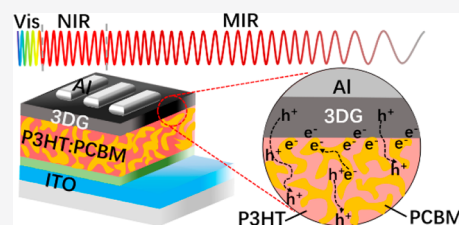
Near-infrared (NIR) and mid-infrared (MIR) light detection play vital roles in thermal imaging, biometrics, and military surveillance. Particularly, MIR detection covers the molecular vibrational regions, which can be employed in gas detection, liquid inspection, and biological tissue identification.[1−6] However, the current NIR and MIR photodetectors are generally made of narrow-bandgap inorganic materials such as Si,[7] GaInAs,[8] HgCdTe alloys,[9] and quantum-well and quantum-dot structure[10−12] that suffer from rigid mechanical property, fabrication technology limitation, and working environments, severely limiting their applications, especially in flexible and wearable electronics.[13−15] Organic semiconductors have attracted tremendous attention owning to intrinsic flexible properties, solution processability, rather tunable bandgap, large-scale roll to roll production, and compatibility with flexible substrate, showing promising applications in next-generation flexible photodetectors for visible light detection.[16−24] However, they generally suffer from large bandgap, weak absorption, and poor charge generation in NIR and MIR regions, resulting in poor performance long-wavelength detection. The gapless two-dimension (2D) single-layer graphene exhibits potential NIR and MIR detection at room temperature because of its unique electronic structure, broad spectra absorption, easy fabrication, and flexibility,[25−27] making it attractive for broadband and flexible photodetectors.[28−32] In the past few years, long-wavelength photodetector based on graphene ($\lambda = 2$ μm),[4,31] HgTe/graphene ($\lambda = 1.55$ μm),[33] PbS/graphene ($\lambda = 1.4$ μm),[34] etc., have been developed by fabricating photo-

conductor and phototransistors. Nonetheless, the practical application is limited by its weak light absorption, large noise, and high dark current of graphene, the stability and toxicity of QDs, and high gating voltage as well as complex structure of phototransistor.[35−37] Very recently, our group have developed a three-dimensional chemical cross-linked graphene (3DG) sponge material with many unique properties from a simple solvothermal process[38] and explored its applications in water treatment,[39] electromagnetic shielding,[40,41] and photodetectors.[42] 3DG sponge, consisting of mass amount almost all edge-linked single layer graphene sheets and behaving as a true bulk graphene material, has high specific surface area and broadband absorption characteristics to make it a good light detection material.[38,39,41] However, 3DG sponge-based photoconductors still suffer from low responsivity as the photogenerated electron−hole pairs cannot be effectively separated. Moreover, thin 3DG has poor mechanical properties and a porous surface, making it difficult to handle and maintain good contact with the electrode. Therefore, it is vital to design devices to enhance the separation and collection of photocarriers in 3DG for NIR and MIR detection.
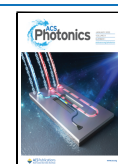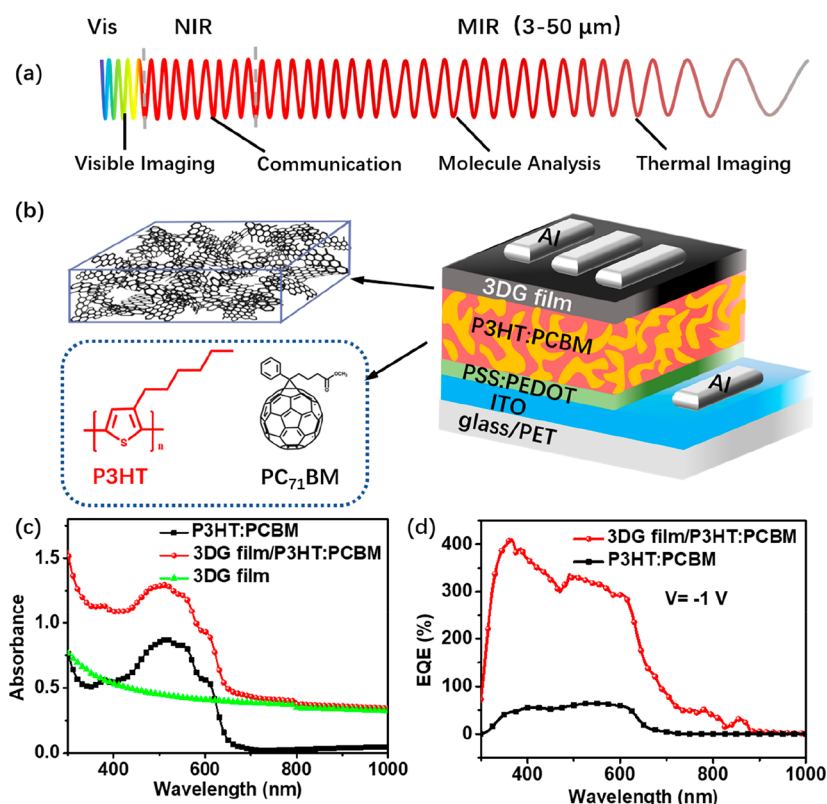
Figure 1. (a) Application fields of photodetectors from visible to MIR spectrum. (b) Schematic of the 3DG film/organic photodetector. (c) UV–Vis–NIR spectra of 3DG film, P3HT:PCBM film, and 3DG film/P3HT:PCBM. (d) EQE curves for P3HT:PCBM photodetector and 3DG film/organic photodetector under illumination at a bias of −1 V.

To achieve NIR and MIR detection with high responsivity, it is crucial to both introduce appropriate materials with efficient NIR and MIR light absorption and design proper devices for also efficient charge separation and transfer. Herein, we reported a flexible Vis–MIR photodetector by using a hybrid layer of both 3DG film and classic [6,6]-phenyl C_{71} butyric acid methyl ester (PCBM) and poly(3-hexylthiophene) (P3HT)-based bulk heterojunction (BHJ) materials in the organic photodetectors. Compared with previous report about graphene/organic material-based devices such as graphene/C60 ($\lambda = 0.8$ μm),[43] graphene/polymer ($\lambda = 2$ μm),[37] and graphene/organic semiconductor ($\lambda = 1.55$ μm),[35] the 3DG/P3HT:PCBM-based hybrid photodetector leads to a broad spectra detection from visible to MIR (10.6 μm) and also excellent responsivity in NIR region (108 A W^{-1} at 1000 nm), which is the longest wavelength ever reported with high performance. Moreover, the hybrid organic photodetectors can detect picowatt-level light with responsivity of 5.8×10^5 A W^{-1}. Significantly, this remarkable and achieved performance in an extremely broad region is mainly contributed to the combination of selected active materials for desired wavelength absorption and the unique device structure for photocarriers separation. Instead of trapping sites caused by the photogating effect in the phototransistor, the PCBM and the functional groups in 3DG in the hybrid device acts as electron trapping sites, leading to high photocurrent gains and responsivity. Furthermore, the 3DG film/organic hybrid photodetectors are compatible with rigid and flexible substrates, showing great potential in wearable devices.

RESULTS AND DISCUSSION

The typical application fields of photodetectors from visible to MIR spectrum display in Figure 1a, such as imaging, communication, chemical analysis, thermal imaging, etc. The specific applications are determined by the spectra range of photodetectors. For example, NIR photodetector is widely utilized in vivo bioimaging due to its strong penetrability in living tissues, which is known as biological window.[44] Some gases such as carbon dioxide, methane, and water have strong absorption in MIR region due to their vibrational resonances with MIR, indicating a series of applications in environmental monitor, health analysis, as well as industry processing.[45,46] As previously reported, photodetectors have been studied by using the classic bulk-heterojunction of P3HT:PCBM as the active layer, but with only good response in the visible range shorter than 650 nm.[47] Considering the wide and efficient light absorption of 3DG from VIS to the microwave band, we thus fabricated a hybrid device using both P3HT:PCBM and 3DG as the active layer materials.[41] By spin-coating PSS: PEDOT and P3HT:PCBM solution on ITO substrate sequentially, we obtain the organic film for visible light detection, followed by transferring 3DG film on organic layer to obtain the hybrid device for wide range coverage. Figure 1b illustrates the chemical structure of P3HT, PCBM, 3DG, and the architecture of the hybrid photodetectors. The 3DG film was prepared via a confined solvothermal reaction in a hydrothermal autoclave as shown in Supporting Information (SI), Figure S1, and the process details are introduced in experimental section.[38] The SEM image displayed in SI, Figure S2, indicates that the surface of the 3DG film has wrinkles due to the collapse of the porous structure during the
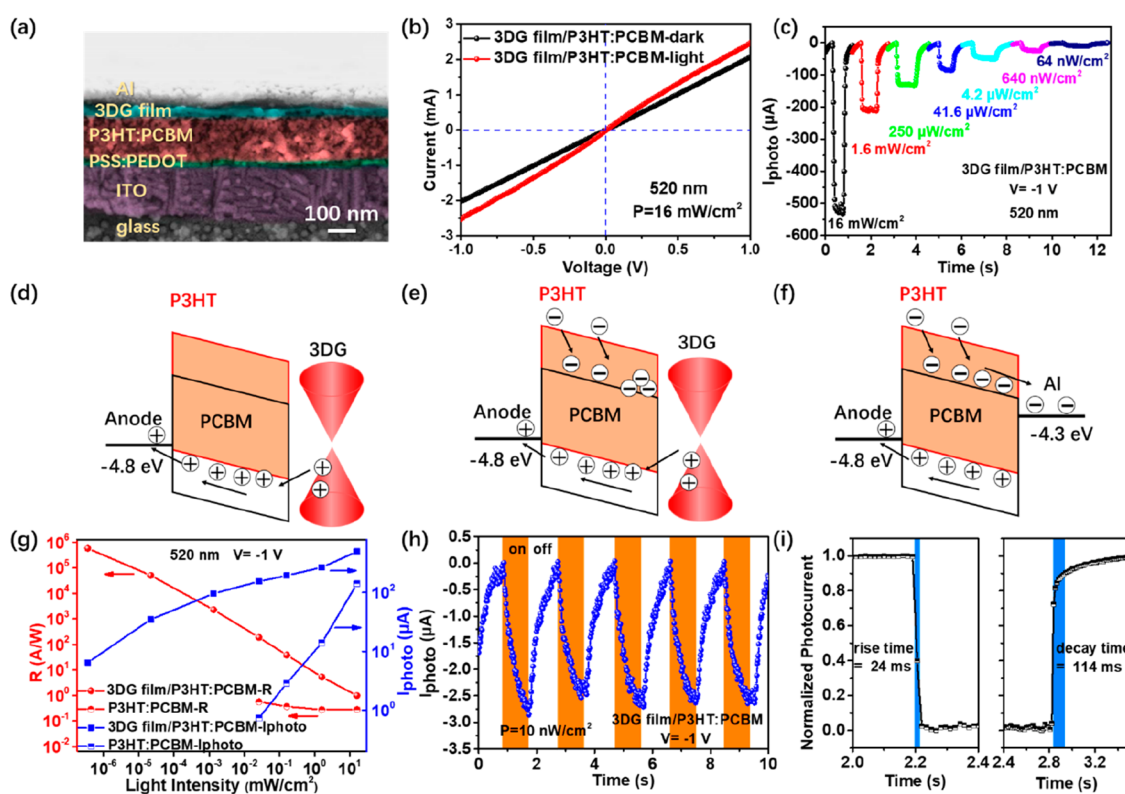
Figure 2. (a) Cross-sectional SEM image of the 3DG film/organic photodetector. (b) $I-V$ response of the 3DG film/organic photodetector in the dark and 520 nm laser illumination (16 mW cm^{-2}). (c) Temporal photoresponse curves of the 3DG film/organic photodetector under 520 nm illumination with different light intensities at -1 V. Working mechanism of the 3DG film/organic photodetector in the dark (d) and under visible illumination (e). (f) Working mechanism of the P3HT:PCBM photodetector under visible illumination. (g) Power-dependent R and I_{photo} under 520 nm laser illumination at -1 V for the 3DG film/organic photodetector and pure organic photodetector. (h) Photoresponse curve of the photodetector under 520 nm light (10 nW cm^{-2}) at -1 V. (i) The response speed of the hybrid device under 520 nm illumination.

drying process, which is further confirmed by SEM images shown in SI, Figure S3. The XRD (SI, Figure S4a), Raman spectrum (SI, Figure S4b), infrared spectroscopy, and XPS spectra (SI, Figure S5) data indicate that graphene oxide sheets are partially reduced and cross-linked to produce a 3D network, maintaining the single-layer structure and intrinsic properties of graphene, which is consistent with our previous report.[38,39] The oxygen-containing functional groups left in 3DG films can act as defect sites to trap photocarriers, enhancing the photoresponsivity of the hybrid device.[48] As shown in Figure 1c, the 3DG film has broadband absorption features in the ultraviolet−visible−infrared region with no characteristic absorption peak, while the P3HT:PCBM absorption is mainly in the visible region from 400 to 650 nm. The absorption of 3DG film/P3HT:PCBM is basically equivalent to the sum of the absorption of these two layers. Therefore, the hybrid active layer, consisting of 3DG and P3HT:PCBM, exhibits a wide and efficient absorption from Vis to IR range. As shown in Figure 1d, the hybrid photodetector presents significantly higher external quantum efficiency (EQE) than the normal P3HT:PCBM-based photodiode at a bias of -1 V in almost the entire visible−NIR region.

Figure 2a is a cross-sectional colored SEM image of the hybrid device corresponding to the schematic diagram of Figure 1b, and the details of device fabrication is depicted in the experimental section. The total thickness of hybrid device is thus less than 250 nm, indicating the ultrathin property of the hybrid device. Figure 2b displays linear current−voltage

$(I-V)$ curves of the 3DG film/organic photodetector both in dark and under illumination of 520 nm laser at 16 mW cm^{-2}, which indicates that the 3DG film/organic photoconductor exhibits the typical photoconductive characteristics. Under light illumination, the response current reaches 500 μA under a bias of -1 V. For comparison, the organic photodetectors based on P3HT:PCBM active layer without 3DG presented in SI, Figure S6, shows nonlinear $I-V$ curve with a rectifying ratio of 410, indicating the photodiode characteristics. Moreover, the responsivity of the device at different wavelength is independent of negative bias (SI, Figure S6d), which is consistent with the photodiode. Figure 2c illustrates the current−time $(I-t)$ curves under various light intensity, showing a stable and repeatable photoresponse of the device. Under visible light (520 nm) irradiation, the hybrid device shows a sharp increase of current owing to the photocarrier generation in active materials. Figure 2d,e present the bandgap diagram and working mechanism of the 3DG film/organic photodetector. As 3DG is a p-type semiconductor due to functional groups at the edge of graphene with a high work function of about 4.9 eV, it can work as hole transport layer.[49−51] PSS:PEDOT and 3DG can both work as a hole transport layer, benefiting the hole transport in organic layers and blocking the electron drift due to the barrier at the interface of electrode and PCBM. Therefore, the hybrid device shows a linear $I-V$ curve in the dark. In the hybrid photodetector, both organic active materials and 3DG contribute to the photocurrent generation. Under visible light irradiation, the excitons generated in organic materials are
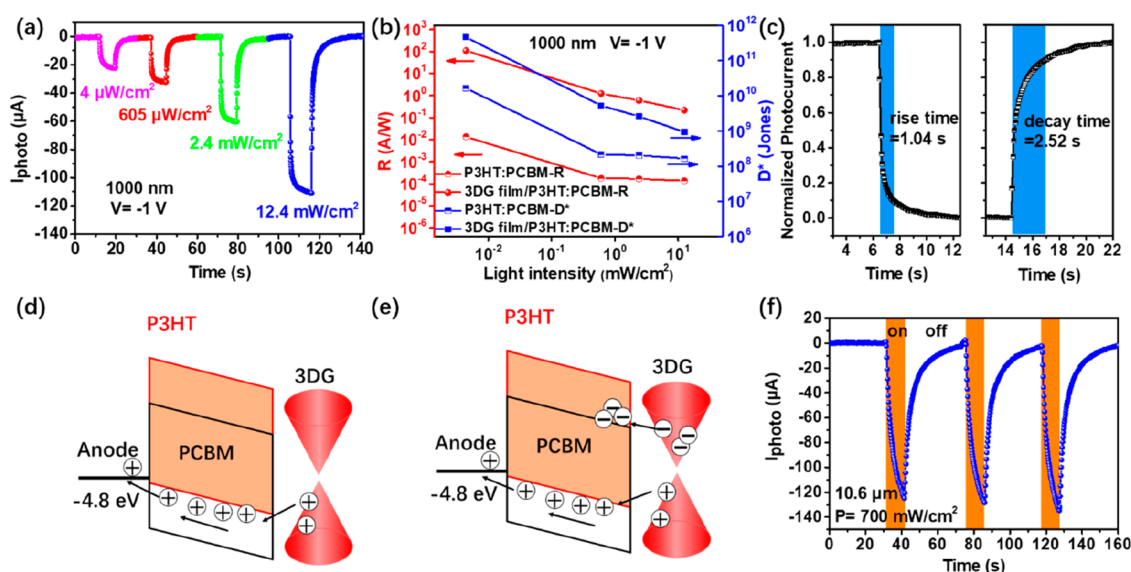
Figure 3. (a) Temporal photoresponse curves of the 3DG film/organic photodetector under 1000 nm illumination with different light intensities at −1 V. (b) Power-dependent R and D^* under 1000 nm laser illumination at −1 V for the 3DG film/organic photodetector and pure organic photodetector. (c) The response speed of the device under 1000 nm illumination. Working mechanism of the 3DG film/organic photodetector in the dark (d) and under infrared illumination (e). (f) Photoresponse curve of the photodetector under 10600 nm laser illumination (700 mW cm^{-2}) at a bias of −1 V.

separated at the interface between the donor and the acceptor due to the built-in electric field to form free carriers, in which photoelectrons transfer from P3HT to PCBM and are trapped in PCBM. The trapped electrons cause n-doping PCBM, which elevates the electron barrier between PCBM and 3DG after Fermi level alignment. Therefore, it is easy to inject holes from 3DG to organic materials under bias due to the decreased barrier thickness.[43,52] Afterward, when excess holes are injected under the induction of an external electric field, they begin to recirculate during the lifetime of trapped electrons, forming an enhanced photocurrent gain and photocurrent response compared with the control device fabricated with P3HT:PCBM (Figure 2e).[53] For the P3HT:PCBM device, the photoelectrons drift from P3HT to PCBM, which are collected by the Al electrode, and holes drift to the opposite direction (Figure 2f). In addition, 3DG can also generate electron−hole pairs under light irradiation due to its semiconductor properties, which has been reported in previous research.[42] The oxygen groups in 3DG can capture electrons to slow down the carrier recombination, prolonging the lifetime of photocarriers and enhancing the photocurrent gain, which is an inevitable and common process in reduced graphene oxide.[54] Moreover, the p-type 3DG can form a built-in electric field with PCBM due to electron and hole diffusion at the interface of 3DG and PCBM, which promotes the separation of electron−hole pairs generated in 3DG and electrons trapped in PCBM.

The responsivity (R) is a measure of the optical-to-electrical conversion efficiency of a photodetector, which is defined as[42]

$$R = \frac{I_{photo}}{P} = \frac{I_{illu} - I_{dark}}{E_e \times A} \tag{1}$$

where I_{illu} and I_{dark} are the current with illumination and in the dark, and P, E_e, and A are the incident light power, the laser irradiance, and the effective illumination area, respectively. Specific detectivity (D^*) is a parameter of a photodetector to

determine the minimum illumination light power, and it can be defined as[55]

$$D^* = \frac{R\sqrt{AB}}{i_n} \tag{2}$$

where A is the effective illumination area, B is the bandwidth, and i_n is the noise current. Assuming that the shot noise is the main contributor to the noise, the formula 2 can be simplified to the formula 3

$$D^* = \frac{RA^{1/2}}{(2eI_{dark})^{1/2}} \tag{3}$$

Here, e is the electron charge.

The responsivity of the hybrid photodetector increases significantly with the decrease of incident light, and the photocurrent shows a nonproportional decay (Figure 2g), which is caused by the photocurrent gain in the 3DG film/P3HT:PCBM hybrid system.[56] In contrast, the photocurrent of the P3HT:PCBM only detector decreases proportionally with the decrease of light intensity (SI, Figure S6b) because of the photodiode characteristics. The responsivity of the hybrid device can reach 5.8×10^5 A W^{-1}, and the specific detectivity can reach 3×10^{15} Jones under the illumination by 520 nm laser with 0.4 nW cm^{-2} of irradiance at the bias voltage of −1 V (Figure 2g, and SI, Figure S7). Furthermore, the linear dynamic range of the hybrid device can reach 117 dB under 520 nm laser illumination, corresponding to a dynamic range of about 6-magnitude (SI, Figure S7c). The photocurrent gain (G) can be calculated using the following formula[56]

$$G = \frac{I_{photo}/e}{P/h\nu} \times \frac{1}{QE} \tag{4}$$

where P is the incident light power, $h\nu$ is the energy per photon, and QE is the quantum efficiency of charge carrier generated per unit photon. Assuming a QE of 1, the maximum value of the photocurrent gain is found to be as high as 1.4 ×
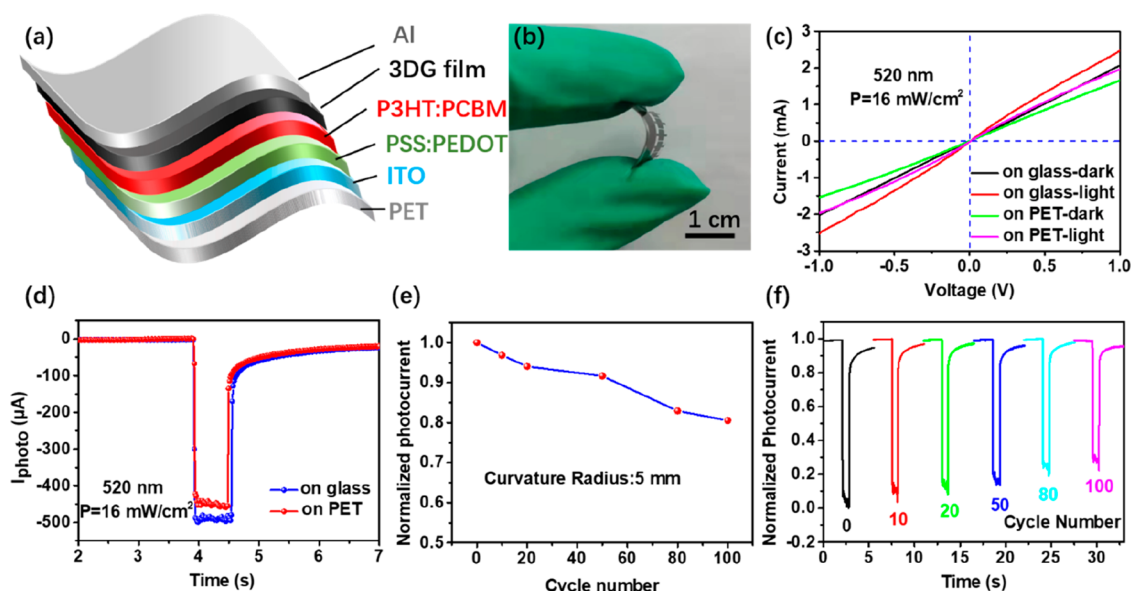
Figure 4. (a) Schematic of the flexible 3DG film/organic photodetector. (b) The optical photo of the bended flexible 3DG film/organic photodetector. (c) $I-V$ response of the rigid and flexible devices in the dark and 520 nm laser illumination (16 mW cm^{-2}). (d) Temporal photoresponse curves of the rigid and flexible devices under 520 nm illumination. (e) Normalized photocurrent for flexible 3DG film/organic photodetector as a function of cycle number of repeated bending to a radius of 5 mm. Inset is the optical image of the bended flexible hybrid photodetector. (f) Photocurrent response curves of flexible devices at different bending cycles.

10^6 with 0.4 nW cm^{-2} of irradiance. Under a weak irradiance of 10 nW cm^{-2} and 1 nW cm^{-2} at 0.5 Hz, the hybrid detector still has high photocurrent response of 2.5 and 0.8 μA, respectively (Figure 2h, and SI, Figure S8). Furthermore, the hybrid detector exhibits a sharp response to incoming photons, and the rise and decay time is found to be 24 and 114 ms, respectively (Figure 2i). The longer decay time is mainly due to the trapping of carriers in PCBM, which leads to prolonged carrier life and slower photocurrent recovery but generate gains and obtain higher responsivity. We also tested the photoelectric response of the hybrid device to 450 and 635 nm laser (SI, Figure S7), and similar results were obtained. This indicates that the hybrid photodetector has excellent responsivity and specific detectivity in the visible light region.

As graphene has broad spectra absorption, long wavelength beyond visible light can excite 3DG to generate photocarriers. Here, we choose 1000 nm wavelength to irradiate the hybrid device to test its performance in NIR region. Figure 3a presents the photoelectric response of the hybrid photodetectors at 1000 nm, showing stable and reliable response and recovery. In the NIR region (e.g., 1000 nm), the responsivity of the hybrid device is 0.6 A W^{-1}, with the incident power is 2.4 mW cm^{-2}, and the responsivity can reach 108 A W^{-1} under weak light of 4 μW cm^{-2} with 4.7×10^{11} Jones of D^*. For comparison, the responsivity of the P3HT:PCBM detector is 4 orders of magnitude lower than that of the hybrid detector (Figure 3a,b, and SI, Figure S9). Therefore, photoresponse in the infrared region mainly owes to the contribution of the 3DG film, and the rise and fall time of the photoresponse of the hybrid photodetector under 1000 nm laser illumination are 1.04 and 2.52 s, respectively (Figure 3c). As mentioned before, under NIR light irradiation, photocarriers are only generated in 3DG due to its narrow bandgap and broad spectra absorption in this region. Some of the photoelectrons are trapped by functional groups in 3DG, slowing the photocarrier recombination and leading to high photocurrent gain. Moreover, 3DG

is p-type semiconductor that can form built-in electric field with PCBM after Fermi level alignment, which benefits the hole−electron pairs separation and electrons are trapped by PCBM. In the hybrid photodetector, the P3HT layer also works as a hole conducting channel. Therefore, holes drift to P3HT under bias while the photoelectrons are trapped in PCBM due to its high electron affinity and captured by functional groups in 3DG, which enhances the separation of photocarriers and the responsivity in the NIR region (Figure 3d,e).[57] To confirm this hypothesis, we prepare a hybrid device without PCBM, which shows no response under NIR irradiation because of few electron traps in 3DG, leading to the recombination of holes and electrons in 3DG. Moreover, the hybrid device without P3HT also shows much weaker response to both visible and NIR light, as there is no hole conducting channel in the device (SI, Figure S10). We also extend the wavelength to MIR region (10.6 μm) with a light intensity of 700 mW cm^{-2}, and the results indicate the device also demonstrates a clear and stable photoresponse (Figure 3f, and SI, Figure S11). This remarkable photoresponse of the hybrid device is owed to both the excellent broadband light absorption of the 3DG film and the unique device structure. SI, Table S1 comparing to the performance of graphene-based infrared photodetectors, indicating that our device shows much broader detection range and higher responsivity in the MIR range.

The introduction of 3DG films has several advantages in the 3DG film/organic hybrid devices. First, as indicated above, 3DG is consisted of mass of amount single layered graphene sheets, and thus it has broadband absorption features from visible to MIR region to achieve the broadband light detection. Second, 3DG films have a porous structure and a surface rich in wrinkles, which can further improve the absorption of light (SI, Figure S12a). Third, 3DG films still retain some oxygen-containing functional groups, which can act as defects to trap the carriers, leading to a high gain and improved responsivity
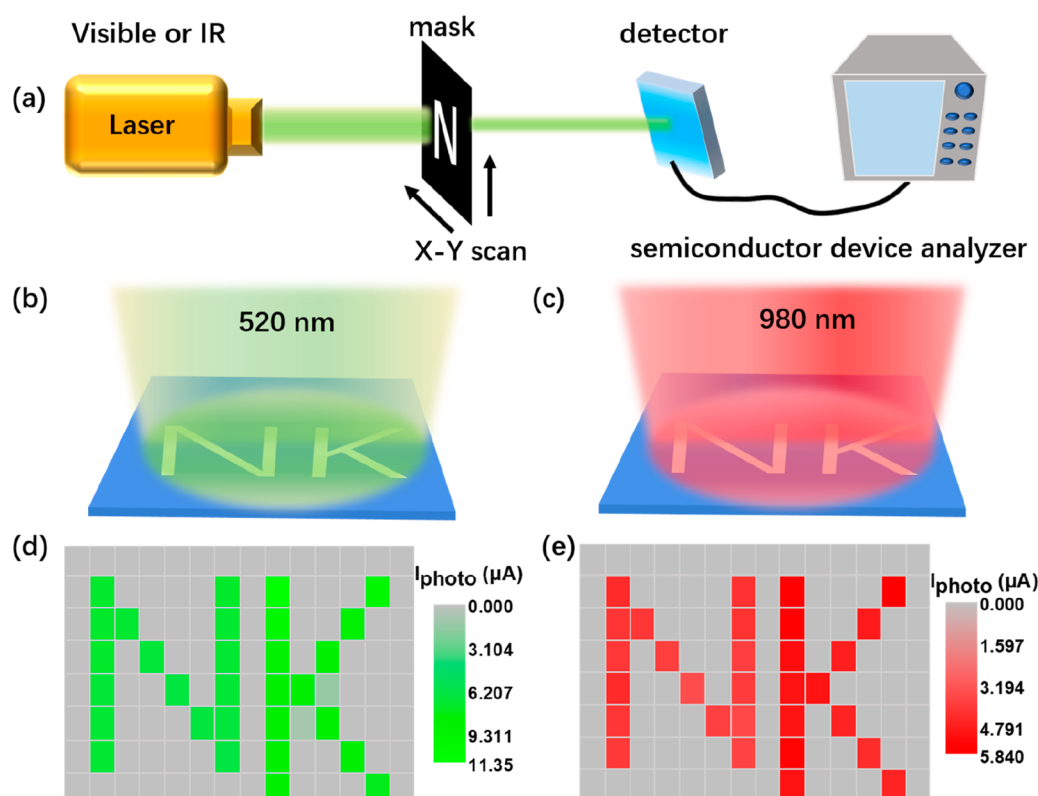
Figure 5. (a) Schematic diagram for the imaging system employing the photodetector as imaging pixel. The diagrams for imaging under 520 nm (b) and 980 nm (c) laser illumination. The imaging results obtained from the imaging system at −1 V under 520 nm (16.8 μW cm^{-2}) (d) and 980 nm (1.1 mW cm^{-2}) (e) laser illumination.

under IR irradiation. Furthermore, the graphene/organic heterojunction structure is also conducive to the separation of electron−hole pairs. Finally, the graphene sheets of the 3DG film are cross-linked with each other instead of $\pi-\pi$ stacking, which means some of the graphene sheets are in line of the vertical direction. This should be beneficial for the transport of carriers in the vertical direction between the two electrodes. Thanks to all these combined factors all these together, our 3DG film/organic broadband hybrid photodetectors thus could present the characteristics of high responsivity, detectivity, broadband detection, and is also capable for the detection of picowatt-level weak light.

Unlike the infrared photodetector based on 2D materials that require sophisticated equipment, such as photolithography and e-beam lithography,[58] organic optoelectronic materials are inherently solution processable and compatible with flexible substrates. Hence, flexible hybrid photodetectors following the same protocol were fabricated using polyethylene terephthalate (PET) as the substrates with the device configuration of PET/ITO/PSS: PEDOT/P3HT:PCBM/3DG film/Al and the optoelectronic properties were investigated as shown in Figure 4. The transmittance of rigid (glass/ITO) and flexible (PET/ITO) substrates at 520 nm is basically same (SI, Figure S12b). The $I-V$ curves of the rigid device and the flexible device are shown in Figure 4c. As the resistivity of the substrate PET/ITO is higher than that of the rigid one, the dark current of the flexible device is slightly lower. Moreover, the response current of the flexible device can maintain more than 90% of the rigid device under 520 nm illumination as plotted in Figure 4d. Electrical and mechanical stability in the bending condition is important in the practical applications of the flexible devices,

and the flexible device we prepared still has a stable photoresponse under bending conditions (SI, Figure S13). We also conducted a bending cycle test on the prepared flexible hybrid photodetector with a bending radius of 5 mm. After 100 bending cycles, the photocurrent of the test sample can still maintain more than 80% of the initial response current (Figure 4e,f).

To assess the practical application of the Vis−NIR−MIR photodetector, we carried out an imaging system for visible and NIR light imaging (Figure 5 and SI, Figure S14). The hollow mask of letters "N" and "K" are mounted on a 2D-translation stage, which is placed between the laser and photodetector, and the semiconductor device analyzer is used to collect photocurrent. Here we use green light (520 nm) and NIR (980 nm) as the laser light source. By moving the mask in horizon and vertical direction with a step of 2 mm, light can penetrate the hollow mask to irradiate the photodetector, which shows a clear image. Therefore, the hybrid device has great potential in bioimaging in the NIR region.

■ CONCLUSION

In conclusion, we report the first design and demonstration of flexible Vis−MIR photodetector by incorporating 3DG film in OPD, which is capable of photodetection from visible to MIR light with ultrahigh responsivity, broad spectra detection, high detectivity, and low detection limit all together. Such wide range has not reported before with such high photoresponse, detectivity, and low detection limit. The remarkable performance of the hybrid device in the IR region is attributed to the broad absorption of 3DG film and the unique device structure, in which the acceptor and the functional groups in 3DG can

trap photogenerated carriers, thereby prolonging the life of carriers and rendering a high gain and high responsivity. Thus, the hybrid device exhibits a high responsivity of 108 A W^{-1} in the NIR region not seen before. In addition, the obtained photoresponsivity can reach 5.8×10^5 A W^{-1} under 520 nm laser illumination, and the device exhibits a good detection capability for lowest picowatt-level weak light. The flexible hybrid detectors can realize large-scale and cost-efficient production with excellent performance and good mechanical stability and opens up an alternative route for wearable electronics.

■ ASSOCIATED CONTENT

ⓢ Supporting Information

The Supporting Information is available free of charge at https://pubs.acs.org/doi/10.1021/acsphotonics.1c01690.

> Detailed of the synthesis and characterization of 3DG films; methods of fabrication of 3DG film/organic hybrid photodetector; temporal photoresponse curves of P3HT:PCBM devices under visible and infrared illumination; power-dependent R and D^* under 450, 520, and 635 nm laser illumination for the 3DG film/ P3HT:PCBM photodetector; the transmittance curves of rigid (glass/ITO) and flexible (PET/ITO) substrate (PDF)

■ AUTHOR INFORMATION

Corresponding Authors

Yongsheng Chen − *The Centre of Nanoscale Science and Technology and Key Laboratory of Functional Polymer Materials, Institute of Polymer Chemistry, College of Chemistry, State Key Laboratory of Elemento-Organic Chemistry, and Renewable Energy Conversion and Storage Center (RECAST), Nankai University, Tianjin 300071, China;* ⓞ orcid.org/0000-0003-1448-8177; Email: yschen99@nankai.edu.cn

Guanghui Li − *The Centre of Nanoscale Science and Technology and Key Laboratory of Functional Polymer Materials, Institute of Polymer Chemistry, College of Chemistry and Renewable Energy Conversion and Storage Center (RECAST), Nankai University, Tianjin 300071, China;* Email: ghli1127@nankai.edu.cn

Authors

Zhen Ge − *The Centre of Nanoscale Science and Technology and Key Laboratory of Functional Polymer Materials, Institute of Polymer Chemistry, College of Chemistry and Renewable Energy Conversion and Storage Center (RECAST), Nankai University, Tianjin 300071, China*

Nuo Xu − *The Centre of Nanoscale Science and Technology and Key Laboratory of Functional Polymer Materials, Institute of Polymer Chemistry, College of Chemistry and Renewable Energy Conversion and Storage Center (RECAST), Nankai University, Tianjin 300071, China*

Yu Zhu − *The Centre of Nanoscale Science and Technology and Key Laboratory of Functional Polymer Materials, Institute of Polymer Chemistry, College of Chemistry and Renewable Energy Conversion and Storage Center (RECAST), Nankai University, Tianjin 300071, China*

Kai Zhao − *The Centre of Nanoscale Science and Technology and Key Laboratory of Functional Polymer Materials, Institute of Polymer Chemistry, College of Chemistry and Renewable Energy Conversion and Storage Center (RECAST), Nankai University, Tianjin 300071, China*

Yanfeng Ma − *The Centre of Nanoscale Science and Technology and Key Laboratory of Functional Polymer Materials, Institute of Polymer Chemistry, College of Chemistry and Renewable Energy Conversion and Storage Center (RECAST), Nankai University, Tianjin 300071, China*

Complete contact information is available at:
https://pubs.acs.org/10.1021/acsphotonics.1c01690

Notes

The authors declare no competing financial interest.

■ ACKNOWLEDGMENTS

■ REFERENCES

(1) Casalino, M.; Sassi, U.; Goykhman, I.; Eiden, A.; Lidorikis, E.; Milana, S.; De Fazio, D.; Tomarchio, F.; Iodice, M.; Coppola, G.; Ferrari, A. C. Vertically Illuminated, Resonant Cavity Enhanced, Graphene-Silicon Schottky Photodetectors. *ACS Nano* **2017**, *11*, 10955−10963.

(2) Papadakis, I.; Stavrou, M.; Bawari, S.; Narayanan, T. N.; Couris, S. Outstanding Broadband (532 nm to 2.2 μm) and Very Efficient Optical Limiting Performance of Some Defect-Engineered Graphenes. *J. Phys. Chem. Lett.* **2020**, *11*, 9515−9520.

(3) Chen, X.; Lu, X.; Deng, B.; Sinai, O.; Shao, Y.; Li, C.; Yuan, S.; Tran, V.; Watanabe, K.; Taniguchi, T.; Naveh, D.; Yang, L.; Xia, F. Widely Tunable Black Phosphorus Mid-Infrared Photodetector. *Nat. Commun.* **2017**, *8*, 1672.

(4) Goossens, S.; Navickaite, G.; Monasterio, C.; Gupta, S.; Piqueras, J. J.; Perez, R.; Burwell, G.; Nikitskiy, I.; Lasanta, T.; Galan, T.; Puma, E.; Centeno, A.; Pesquera, A.; Zurutuza, A.; Konstantatos, G.; Koppens, F. Broadband Image Sensor Array Based on Graphene-CMOS Integration. *Nat. Photonics* **2017**, *11*, 366−371.

(5) Casalino, M. Silicon Meets Graphene for a New Family of near-Infrared Schottky Photodetectors. *Appl. Sci.* **2019**, *9*, 3677.

(6) Telford, W. G. Near Infrared Lasers in Flow Cytometry. *Methods* **2015**, *82*, 12−20.

(7) Sun, X.; Zhang, T.; Yu, L.; Xu, L.; Wang, J. Three-Dimensional a-Si/a-Ge Radial Heterojunction near-Infrared Photovoltaic Detector. *Sci. Rep.* **2019**, *9*, 19752.

(8) Gin, A.; Movaghar, B.; Razeghi, M.; Brown, G. J. Infrared Detection from GaInAs/InP Nanopillar Arrays. *Nanotechnology* **2005**, *16*, 1814−1820.

(9) Rogalski, A. HgCdTe Infrared Detector Material: History, Status and Outlook. *Rep. Prog. Phys.* **2005**, *68*, 2267−2336.

(10) Downs, C.; Vandervelde, T. E. Progress in Infrared Photo-detectors since 2000. *Sensors* **2013**, *13*, 5054−5098.

(11) Rogalski, A. Quantum Well Photoconductors in Infrared Detector Technology. *J. Appl. Phys.* **2003**, *93*, 4355−4391.

(12) Martyniuk, P.; Rogalski, A. Quantum-Dot Infrared Photo-detectors: Status and Outlook. *Prog. Quantum Electron.* **2008**, *32*, 89−120.

(13) Chow, P. C. Y.; Someya, T. Organic Photodetectors for Next-Generation Wearable Electronics. *Adv. Mater.* **2020**, *32*, 1902045.

(14) García de Arquer, F. P.; Armin, A.; Meredith, P.; Sargent, E. H. Solution-Processed Semiconductors for Next-Generation Photo-detectors. *Nat. Rev. Mater.* **2017**, *2*, 16100.

(15) Litvin, A. P.; Martynenko, I. V.; Purcell-Milton, F.; Baranov, A. V.; Fedorov, A. V.; Gun'ko, Y. K. Colloidal Quantum Dots for Optoelectronics. *J. Mater. Chem. A* **2017**, *5*, 13252−13275.

(16) Jin, Z.; Zhou, Q.; Mao, P.; Li, H.; Wang, J. All-Solution-Processed PIN Architecture for Ultra-Sensitive and Ultra-Flexible Organic Thin Film Photodetectors. *Sci. China: Chem.* **2016**, *59*, 1258−1263.

(17) Li, L.; Zhang, F.; Wang, J.; An, Q.; Sun, Q.; Wang, W.; Zhang, J.; Teng, F. Achieving EQE of 16,700% in P3HT:PC$_{71}$BM Based Photodetectors by Trap-Assisted Photomultiplication. *Sci. Rep.* **2015**, *5*, 9181.

(18) Lv, L.; Dang, W.; Wu, X.; Chen, H.; Wang, T.; Qin, L.; Wei, Z.; Zhang, K.; Shen, G.; Huang, H. Flexible Short-Wave Infrared Image Sensors Enabled by High-Performance Polymeric Photodetectors. *Macromolecules* **2020**, *53*, 10636−10643.

(19) Tian, P.; Tang, L.; Xiang, J.; Sun, Z.; Ji, R.; Lai, S. K.; Lau, S. P.; Kong, J.; Zhao, J.; Yang, C.; Li, Y. Solution Processable High-Performance Infrared Organic Photodetector by Iodine Doping. *RSC Adv.* **2016**, *6*, 45166−45171.

(20) Jin, Z.; He, D.; Zhou, Q.; Mao, P.; Ding, L.; Wang, J. Bilayer Heterostructured PThTPTI/WS$_2$ Photodetectors with High Thermal Stability in Ambient Environment. *ACS Appl. Mater. Interfaces* **2016**, *8*, 33043−33050.

(21) Li, W.; Xu, Y.; Meng, X.; Xiao, Z.; Li, R.; Jiang, L.; Cui, L.; Zheng, M.; Liu, C.; Ding, L.; Lin, Q. Visible to near-Infrared Photodetection Based on Ternary Organic Heterojunctions. *Adv. Funct. Mater.* **2019**, *29*, 1808948.

(22) Li, L.; Chen, H.; Fang, Z.; Meng, X.; Zuo, C.; Lv, M.; Tian, Y.; Fang, Y.; Xiao, Z.; Shan, C.; Xiao, Z.; Jin, Z.; Shen, G.; Shen, L.; Ding, L. An Electrically Modulated Single-Color/Dual-Color Imaging Photodetector. *Adv. Mater.* **2020**, *32*, 1907257.

(23) Lan, Z.; Lau, Y. S.; Wang, Y.; Xiao, Z.; Ding, L.; Luo, D.; Zhu, F. Filter-Free Band-Selective Organic Photodetectors. *Adv. Opt. Mater.* **2020**, *8*, 2001388.

(24) Liu, J.; Wang, J.; Wen, H.; Bao, Q.; Shen, L.; Ding, L. Organic Photodetectors: Materials, Structures, and Challenges. *Sol. RRL* **2020**, *4*, 2000139.

(25) Geim, A. K.; Novoselov, K. S. The Rise of Graphene. *Nat. Mater.* **2007**, *6*, 183−191.

(26) Novoselov, K. S.; Geim, A. K.; Morozov, S. V.; Jiang, D.; Zhang, Y.; Dubonos, S. V.; Grigorieva, I. V.; Firsov, A. A. Electric Field Effect in Atomically Thin Carbon Films. *Science* **2004**, *306*, 666−669.

(27) Liu, Y.; Wang, F.; Wang, X.; Wang, X.; Flahaut, E.; Liu, X.; Li, Y.; Wang, X.; Xu, Y.; Shi, Y.; Zhang, R. Planar Carbon Nanotube-Graphene Hybrid Films for High-Performance Broadband Photodetectors. *Nat. Commun.* **2015**, *6*, 8589.

(28) Abid; Sehrawat, P.; Julien, C. M.; Islam, S. S. WS$_2$ Quantum Dots on E-Textile as a Wearable UV Photodetector: How Well Reduced Graphene Oxide Can Serve as a Carrier Transport Medium? *ACS Appl. Mater. Interfaces* **2020**, *12*, 39730−39744.

(29) Ito, Y.; Zhang, W.; Li, J.; Chang, H.; Liu, P.; Fujita, T.; Tan, Y.; Yan, F.; Chen, M. 3D Bicontinuous Nanoporous Reduced Graphene Oxide for Highly Sensitive Photodetectors. *Adv. Funct. Mater.* **2016**, *26*, 1271−1277.

(30) Konstantatos, G.; Badioli, M.; Gaudreau, L.; Osmond, J.; Bernechea, M.; Garcia de Arquer, F. P.; Gatti, F.; Koppens, F. H. Hybrid Graphene-Quantum Dot Phototransistors with Ultrahigh Gain. *Nat. Nanotechnol.* **2012**, *7*, 363−368.

(31) Kang, P.; Wang, M. C.; Knapp, P. M.; Nam, S. Crumpled Graphene Photodetector with Enhanced, Strain-Tunable, and Wavelength-Selective Photoresponsivity. *Adv. Mater.* **2016**, *28*, 4639−4645.

(32) Yang, H. Y.; Lee, H. J.; Jun, Y.; Yun, Y. J. Broadband Photoresponse of Flexible Textured Reduced Graphene Oxide Films. *Thin Solid Films* **2020**, *697*, 137785.

(33) Noumbe, U. N.; Greboval, C.; Livache, C.; Chu, A.; Majjad, H.; Parra Lopez, L. E.; Mouafo, L. D. N.; Doudin, B.; Berciaud, S.; Chaste, J.; Ouerghi, A.; Lhuillier, E.; Dayen, J. F. Reconfigurable 2D/0D P-N Graphene/HgTe Nanocrystal Heterostructure for Infrared Detection. *ACS Nano* **2020**, *14*, 4567−4576.

(34) Yousefi, R.; Mahmoudian, M. R.; Sa'aedi, A.; Cheraghizade, M.; Jamali-Sheini, F.; Azarang, M. Effect of Annealing Temperature and Graphene Concentrations on Photovoltaic and NIR-Detector Applications of PbS/RGO Nanocomposites. *Ceram. Int.* **2016**, *42*, 15209−15216.

(35) Han, J.; Wang, J.; Yang, M.; Kong, X.; Chen, X.; Huang, Z.; Guo, H.; Gou, J.; Tao, S.; Liu, Z.; Wu, Z.; Jiang, Y.; Wang, X. Graphene/Organic Semiconductor Heterojunction Phototransistors with Broadband and Bi-Directional Photoresponse. *Adv. Mater.* **2018**, *30*, 1804020.

(36) Cui, M.; Guo, Y.; Zhu, Y.; Liu, H.; Wen, W.; Wu, J.; Cheng, L.; Zeng, Q.; Xie, L. Graphene-Organic Two-Dimensional Charge-Transfer Complexes: Intermolecular Electronic Transitions and Broadband near-Infrared Photoresponse. *J. Phys. Chem. C* **2018**, *122*, 7551−7556.

(37) Iqbal, M. A.; Liaqat, A.; Hussain, S.; Wang, X.; Tahir, M.; Urooj, Z.; Xie, L. Ultralow-Transition-Energy Organic Complex on Graphene for High-Performance Shortwave Infrared Photodetection. *Adv. Mater.* **2020**, *32*, 2002628.

(38) Wu, Y.; Yi, N.; Huang, L.; Zhang, T.; Fang, S.; Chang, H.; Li, N.; Oh, J.; Lee, J. A.; Kozlov, M.; Chipara, A. C.; Terrones, H.; Xiao, P.; Long, G.; Huang, Y.; Zhang, F.; Zhang, L.; Lepro, X.; Haines, C.; Lima, M. D.; Lopez, N. P.; Rajukumar, L. P.; Elias, A. L.; Feng, S.; Kim, S. J.; Narayanan, N. T.; Ajayan, P. M.; Terrones, M.; Aliev, A.; Chu, P.; Zhang, Z.; Baughman, R. H.; Chen, Y. Three-Dimensionally Bonded Spongy Graphene Material with Super Compressive Elasticity and near-Zero Poisson's Ratio. *Nat. Commun.* **2015**, *6*, 6141.

(39) Yang, Y.; Zhao, R.; Zhang, T.; Zhao, K.; Xiao, P.; Ma, Y.; Ajayan, P. M.; Shi, G.; Chen, Y. Graphene-Based Standalone Solar Energy Converter for Water Desalination and Purification. *ACS Nano* **2018**, *12*, 829−835.

(40) Chen, H.; Huang, Z.; Huang, Y.; Zhang, Y.; Ge, Z.; Ma, W.; Zhang, T.; Wu, M.; Xu, S.; Fan, F.; Chang, S.; Chen, Y. Consecutively Strong Absorption from Gigahertz to Terahertz Bands of a Monolithic Three-Dimensional Fe$_3$O$_4$/Graphene Material. *ACS Appl. Mater. Interfaces* **2019**, *11*, 1274−1282.

(41) Zhang, Y.; Huang, Y.; Zhang, T.; Chang, H.; Xiao, P.; Chen, H.; Huang, Z.; Chen, Y. Broadband and Tunable High-Performance Microwave Absorption of an Ultralight and Highly Compressible Graphene Foam. *Adv. Mater.* **2015**, *27*, 2049−2053.

(42) Li, Y.; Zhang, Y.; Yu, Y.; Chen, Z.; Li, Q.; Li, T.; Li, J.; Zhao, H.; Sheng, Q.; Yan, F.; Ge, Z.; Ren, Y.; Chen, Y.; Yao, J. Ultraviolet-to-Microwave Room-Temperature Photodetectors Based on Three-Dimensional Graphene Foams. *Photonics Res.* **2020**, *8*, 368−374.

(43) Qin, S.; Jiang, H.; Du, Q.; Nie, Z.; Wang, X.; Wang, W.; Wang, X.; Xu, Y.; Shi, Y.; Zhang, R.; Wang, F. Planar Graphene-C$_{60}$-Graphene Heterostructures for Sensitive UV-Visible Photodetection. *Carbon* **2019**, *146*, 486−490.

(44) Guo, Z.; Park, S.; Yoon, J.; Shin, I. Recent Progress in the Development of near-Infrared Fluorescent Probes for Bioimaging Applications. *Chem. Soc. Rev.* **2014**, *43*, 16−29.

(45) Kim, S.-S.; Young, C.; Vidakovic, B.; Gabram-Mendola, S. G. A.; Bayer, C. W.; Mizaikoff, B. Potential and Challenges for Mid-Infrared Sensors in Breath Diagnostics. *IEEE Sens. J.* **2010**, *10*, 145−158.

(46) Fedeli, J.-M.; Nicoletti, S. Mid-Infrared (Mid-IR) Silicon-Based Photonics. *Proc. IEEE* **2018**, *106*, 2302−2312.

(47) Yasin, M.; Tauqeer, T.; Karimov, K. S.; San, S. E.; Kösemen, A.; Yerli, Y.; Tunc, A. V. P3HT:PCBM Blend Based Photo Organic Field Effect Transistor. *Microelectron. Eng.* **2014**, *130*, 13−17.

(48) Chang, H.; Sun, Z.; Saito, M.; Yuan, Q.; Zhang, H.; Li, J.; Wang, Z.; Fujita, T.; Ding, F.; Zheng, Z.; Yan, F.; Wu, H.; Chen, M.; Ikuhara, Y. Regulating Infrared Photoresponses in Reduced Graphene Oxide Phototransistors by Defect and Atomic Structure Control. *ACS Nano* **2013**, *7*, 6310−6320.

(49) Wang, F.; Endo, M.; Mouri, S.; Miyauchi, Y.; Ohno, Y.; Wakamiya, A.; Murata, Y.; Matsuda, K. Highly Stable Perovskite Solar

Cells with an All-Carbon Hole Transport Layer. *Nanoscale* **2016**, *8*, 11882−11888.

(50) Li, D.; Cui, J.; Li, H.; Huang, D.; Wang, M.; Shen, Y. Graphene Oxide Modified Hole Transport Layer for $CH_3NH_3PbI_3$ Planar Heterojunction Solar Cells. *Sol. Energy* **2016**, *131*, 176−182.

(51) Capasso, A.; Salamandra, L.; Faggio, G.; Dikonimos, T.; Buonocore, F.; Morandi, V.; Ortolani, L.; Lisi, N. Chemical Vapor Deposited Graphene-Based Derivative as High-Performance Hole Transport Material for Organic Photovoltaics. *ACS Appl. Mater. Interfaces* **2016**, *8*, 23844−23853.

(52) Tan, W.-C.; Shih, W.-H.; Chen, Y. F. A Highly Sensitive Graphene-Organic Hybrid Photodetector with a Piezoelectric Substrate. *Adv. Funct. Mater.* **2014**, *24*, 6818−6825.

(53) Liu, J.; Liang, Q.; Zhao, R.; Lei, S.; Hu, W. Application of Organic-Graphene Hybrids in High Performance Photodetectors. *Mater. Chem. Front.* **2020**, *4*, 354−368.
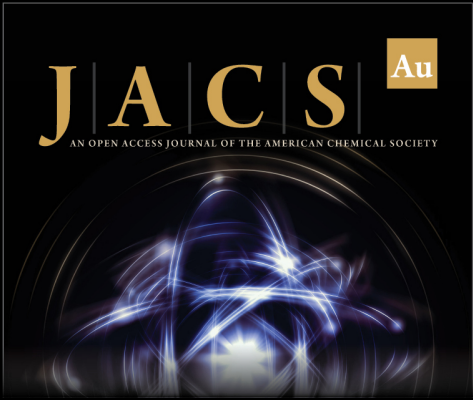
(54) Cao, Y.; Yang, H.; Zhao, Y.; Zhang, Y.; Ren, T.; Jin, B.; He, J.; Sun, J.-L. Fully Suspended Reduced Graphene Oxide Photodetector with Annealing Temperature-Dependent Broad Spectral Binary Photoresponses. *ACS Photonics* **2017**, *4*, 2797−2806.

(55) Chen, Y.; Zheng, Y.; Jiang, Y.; Fan, H.; Zhu, X. Carbon-Bridged 1,2-Bis(2-Thienyl)Ethylene: An Extremely Electron Rich Dithiophene Building Block Enabling Electron Acceptors with Absorption above 1000 nm for Highly Sensitive NIR Photodetectors. *J. Am. Chem. Soc.* **2021**, *143*, 4281−4289.

(56) Bera, K. P.; Haider, G.; Usman, M.; Roy, P. K.; Lin, H.-I.; Liao, Y.-M.; Inbaraj, C. R. P.; Liou, Y.-R.; Kataria, M.; Lu, K.-L.; Chen, Y.-F. Trapped Photons Induced Ultrahigh External Quantum Efficiency and Photoresponsivity in Hybrid Graphene/Metal-Organic Framework Broadband Wearable Photodetectors. *Adv. Funct. Mater.* **2018**, *28*, 1804802.

(57) Shen, L.; Fang, Y.; Wei, H.; Yuan, Y.; Huang, J. A Highly Sensitive Narrowband Nanocomposite Photodetector with Gain. *Adv. Mater.* **2016**, *28*, 2043−2048.

(58) Koppens, F. H. L.; Mueller, T.; Avouris, P.; Ferrari, A. C.; Vitiello, M. S.; Polini, M. Photodetectors Based on Graphene, Other Two-Dimensional Materials and Hybrid Systems. *Nat. Nanotechnol.* **2014**, *9*, 780−793.